Kinetic studies of Ni(II) ions adsorption from aqueous solutions using the blast furnace slag (BF slag)

Toufik Chouchane[*] ⓘ, Ouahida Khireddine and Atmen Boukari

* Correspondence:
chouchane_toufik@yahoo.fr; t.
chouchane@crti.dz
Research Center in Industrial
Technologies CRTI, P.O. Box 64,
Cheraga, 16014 Algiers, Algeria

Abstract

In this work, we used the blast furnace slag for the nickel adsorption in aqueous solution. The physico-chemical characterization showed that the BF slag consists mainly of the silica, lime, and alumina. The specific surface area of the BF slag grains is of the order of 275.8 m^2/g. The optimum elimination parameters are the agitation speed 200 rpm, pH 4.5, the adsorption temperature 20 °C, and particle size between 200 and 500 μm. The adsorption capacity and the efficiency of nickel removal by the BF slag after 90 min of agitation are respectively 53.58 mg/g and 92.7%.

The experimental adsorption data showed that the pseudo-second-order model was the most appropriate in nickel adsorption kinetics; the adsorption isotherm could be described well by the Langmuir model indicating that the process was monolayer, and intra-particle diffusion is not the sole mechanism involved in this process. Thermodynamic study showed that the Ni(II) elimination by BF slag process is spontaneous, exothermic, and less entropic.

Keywords: Slag, Nickel, Adsorption, Water, Kinetics

Introduction

Water is an essential resource for man and his environment; for this reason, its contamination has become one of the challenges that the world must meet for its well-being [1–3]. Indeed, the presence of strong industrialization, the multiplication of urbanization, and non-compliance with regulations regarding discharges has had an alarming impact on water quality [4]. Heavy metals, dyes, organic matter, and biocides are among the pollutants of major concern [5]. Heavy metal ions are among the most released contaminants, and for this reason, they are particularly worrisome [6]. Heavy metals are not biodegradable; therefore, they tend to bioaccumulate, which is their overtime increase of concentration in living organisms [1, 2, 7].

Hence, it is unavoidable to remove the metal ions from water environment by efficient and rigorous methods such as chemical precipitation [8], coagulation/flotation [9], membrane technologies [10], ion exchange [11], electrochemical technologies [12], and adsorption phenomenon [13–16]. Among these techniques, adsorption is still

considered as one of the better technique used to eliminate metal ions from aqueous medium because of its simple operation, high efficiency, and low cost [17, 18]. In this work, we discuss the possibility of eliminating the nickel contained in water by adsorption phenomenon using the slag from the blast furnace (BF) of the El-Hadjar Annaba/ Algeria complex as an adsorbent. BF slag is a solid waste material which is by product of steel making industry; this co-product is formed during the development of cast iron from iron ores. In the world, the annual BF slag production produced is in the tens of million tons, which represents a real environmental problem [19, 20]. From to the literature, many researchers have demonstrated the effectiveness of blast furnace slag in the area of adsorption in solution [21, 22]. Nickel is considered among the most toxic elements of the heavy metals, as it is not biodegradable and thus considered as a risk factor for human health [20, 21]. The main sources of nickel are the industrial discharges from diffuse agricultural, metallurgy, oil refining, exploitation of mineral deposits, electroplating, paint formulation, and the battery manufacturer. In this work, the analyses by X-ray fluorescence, the analyses by X-ray diffraction, and the measurement of the specific surface area by BET method of slag were realized. Furthermore, the contact time, stirring speed, pH, temperature, particle size, and initial concentration were done to evaluate the removal efficiency of the nickel by BF slag as an adsorbent. Adsorption isotherms were presented by Langmuir and Freundlich models. Adsorption kinetic was utilized to describe the kinetics and mechanisms of adsorption process. The thermodynamic parameters were investigated to study the energy exchanges. The purpose of this work is to present a reliable adsorbent at reasonable prices to contribute at the birth of a venerable and sustainable environment.

Methods/experiment

Treatment of BF slag

The samples of the BF slag were collected at the El-Hadjar steel complex Annaba/ Algeria, in the form of rocks and dark color. The washing performed at the crude slag is represented as follows:

- The considered BF slag samples were washed with distilled water and air dried for 48 h
- From an automatic grinder, the washed samples were grinded according to our request: 200, 300, 400, and 500 μm
- The crushed samples were sieved with different the particle sizes (200, 300, 400, and 500 μm)
- Samples with different grain sizes were separated, washed with distilled water, steamed at 105 °C, and stored in plastic boxes

Analytic methods

The nickel concentration was measured by atomic absorption spectroscopy method (PerkinElmer 3110) equipment. The pH of solution was adjusted with a digital pH meter (Hanna Instruments). The characterization was carried out by X-ray fluorescence (Siemens SRS 3000) and X-ray diffraction (Rigaku Ultim IV). The grinding of the slag was carried out by a planetary crusher (Fritsch pulverisette 7 premium line).

The specific surface areas of the BF slag particles were obtained by using the nitrogen gas adsorption-desorption method. The isotherm data for nitrogen gas desorption at 77K were analyzed with the Brunauer, Emmett et Teller model (model BET).

Adsorption protocol

A series of batch experiments were conducted to study the kinetics, mechanism, isotherms, and thermodynamic parameters in the nickel adsorption in solution by BF slag. The study of adsorption kinetics was carried out by adding 1 g of BF slag in aqueous solutions prepared with low nickel nitrate ($Ni(NO_3)_2$, $6H_2O$) in 1 l capacity beakers. The continuous mixing of the solution was ensured during all the tests by mechanical stirrer at different speeds. The temperature was controlled with a water bath equipped with a thermostat. The pH solution was fixed in desired value adding a few drops of concentrated ammonia. The adsorption kinetics were followed by a 5-ml sample using a graduated pipette fitted with a paper filter every 10 min. The samples taken were stocked in flasks, and the concentration of Ni (II) ions was measured using atomic absorption spectrometry (AAS). The experimental protocol was carried out on 04 identical workstations. Two samples were taken from each station to maintain the same concentration. The 04 workstations started at the same time in order to ensure continuity and respect the agitation time. After each two samples, the solution containing nickel and slag is replaced with another identical one. It is obvious that the agitation time is respected and goes in the continuity.

The amounts of adsorbed Ni (II) ions at equilibrium (qe) and at time t (q_t) were calculated from the mass balance expression given by:

$$q_e = \frac{C_0 - C_e}{m} \times V \tag{1}$$

$$q_t = \frac{C_0 - C_t}{m} \times V \tag{2}$$

where C_0 is Initial solute concentration (mg/L), C_e is the residual solute concentration at equilibrium (mg/L), C_t is the residual solute concentration at time t (mg/L), V is the volume of the solution (L), and m is the mass of adsorbent (g).

Results and discussion

Characterization of BF slag

The chemical composition of BF slag is reported in Table 1, where we find a dominance of the SiO_2 (41.1%), CaO (37.2%), and Al_2O_3 (8.2%). The remaining oxides represent relatively low levels (Fe_2O_3, NiO, MgO, K_2O, Na_2O).

Figure 1 represents the diffractogram of blast furnace slag sample from the El-Hadjar complex. The investigations carried out showed that the slag principally lime contains silica and at lesser degree of alumina. This observation justified the results obtained by X-ray fluorescence. The result of the investigations has shown that the specific surface is 275.8 $m^2 \cdot g^{-1}$.

Table 1 Chemical composition of BF slag

| Element	% Mass
CaO	37.2
Al_2O_3	8.2
SiO_2	41.1
Fe_2O_3	2.51
MgO	3.12
NiO	2.64
K_2O	0.3
Na_2O	0.7
P.A.F	4.23

Adsorption study

Determination of adsorption equilibrium time

To determine the pseudo-equilibrium of the nickel adsorption of the blast furnace slag, we varied the time interval from 0 to 300 min. Figure 2 showed the impact of the contact time on the adsorption capacity of nickel in solution beneath our experimental conditions: C_0 30 mg/L, $V_{ag.}$ 200 rpm, pH 5.3, T 20 °C, qe_{exp} 400 μm, and M_{solid} 1 g.

According to kinetic study of the Ni(II) adsorption, we have noticed that the shape of the curve is subdivided into three phases: fast phase, slow phase, and permanent phase (Fig. 2).

For the first phase which varies from 0 to 50 min, the nickel elimination efficacy is very elevated; this is due to the numbers of adsorption vacant sites and probably to the specific surface of the blast furnace slag which could be negatively charged (adsorption under the effect of electrostatic attraction) [23–26]. On the other hand, for the second phase (50 to 90 min) the adsorption efficiency gradually decreases since the vacant sites are not as available.
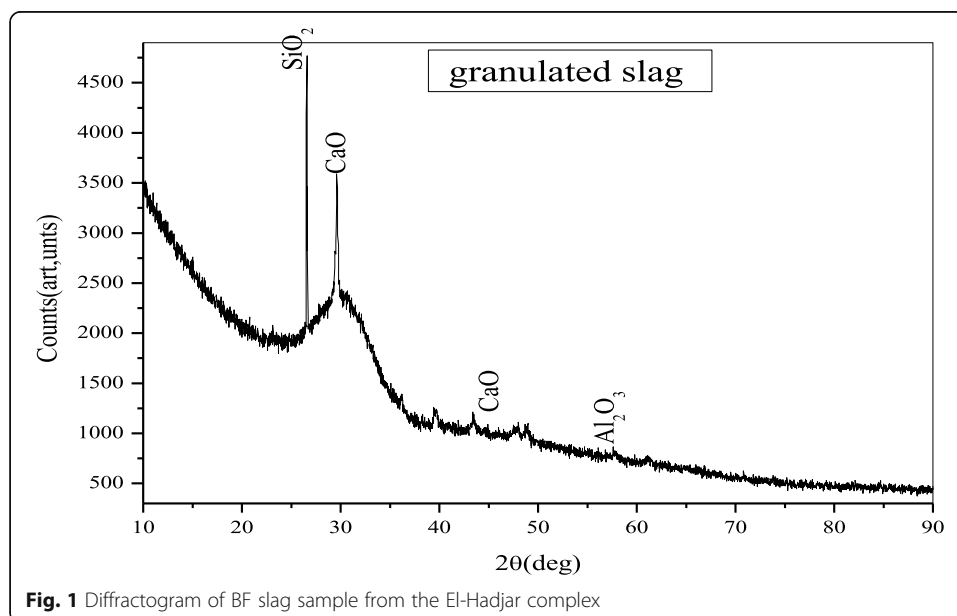
Fig. 1 Diffractogram of BF slag sample from the El-Hadjar complex

**Fig. 2.** Residual concentration of Ni (II) as function of time
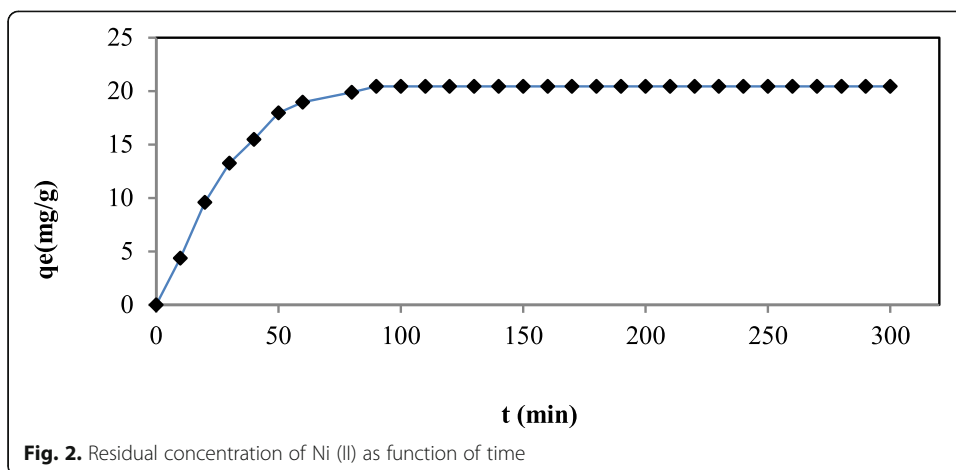
During the last phase, the adsorption capacity has become constant. This means that the adsorbent has reached the saturation phase. For this purpose, we consider 90 min as the equilibrium contact time [27, 28].

Effect of initial pH

The pH of the solution is an important parameter in the adsorption phenomenon because it affects the form of metal in solution, as well as the surface properties of the adsorbent [29, 30]. In this work, three different media were used: pH 2, pH 4.5, and pH 5.3; C_0 30 mg/L; $V_{ag.}$ 200 rpm; T 20 °C; qe_{exp} 400 μm; and M_{solid} 1 g. (Fig. 3).

The kinetic study showed at pH 2 the adsorption is unfavorable (Figs. 3 and 4). At low initial pH value, competition is observed between H^+ ions and Ni^{++} ions in the solution a given that the ionic radius of hydrogen ions is much smaller than the ionic radius of nickel ions. Therefore, it is for this reason that hydrogen ions are the most adsorbed [31, 32].

As the initial pH increased from pH 2 to pH 4.5, the adsorption capacity increased from 12.91 to 23.48 mg/g, and the yield increased from 43.03 to 78.26% (Figs. 3 and 4). Indeed, the efficiency of adsorption can be explained by the effect that the pH of the solution has favorably influenced the surface charges of adsorbent [33]. Moreover, when the initial pH equals 5.3, the nickel ions precipitated owing to augmentation in

Fig. 3 Effect of initial pH

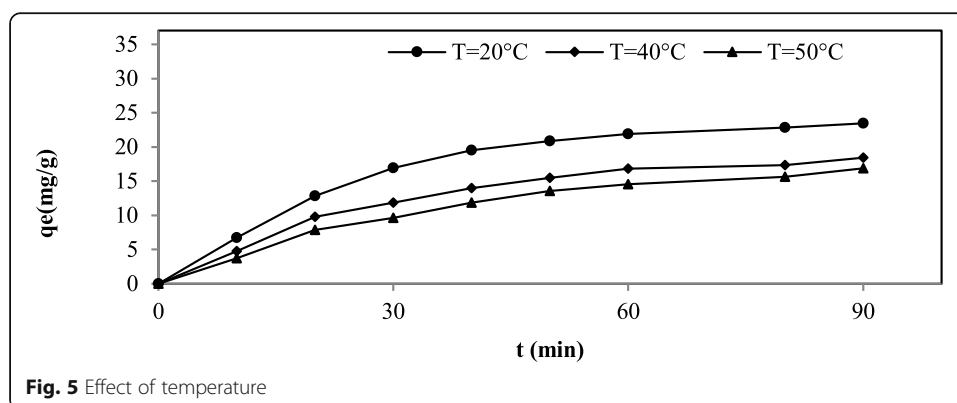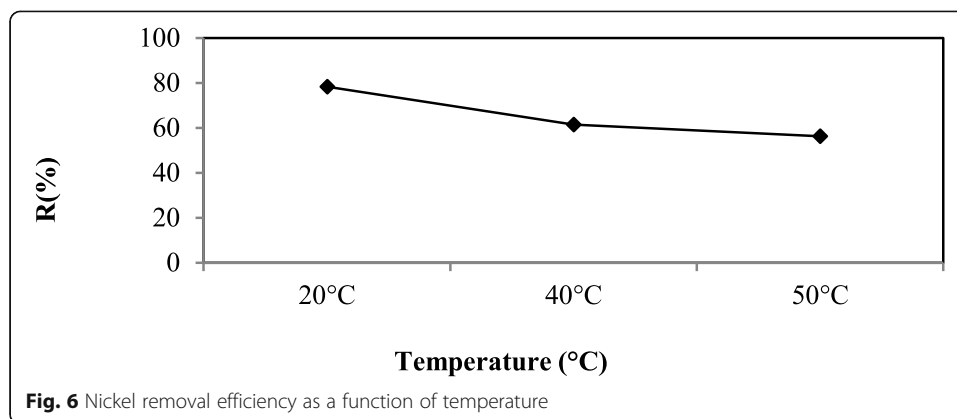**Fig. 4** Nickel removal efficiency as a function of pH
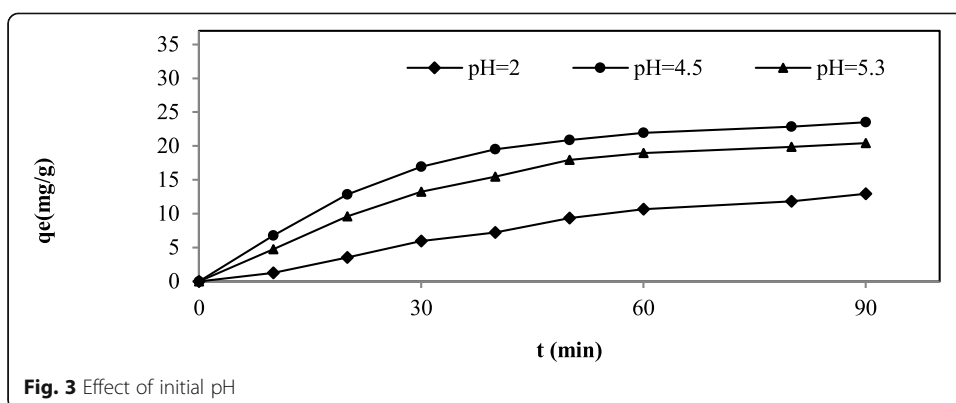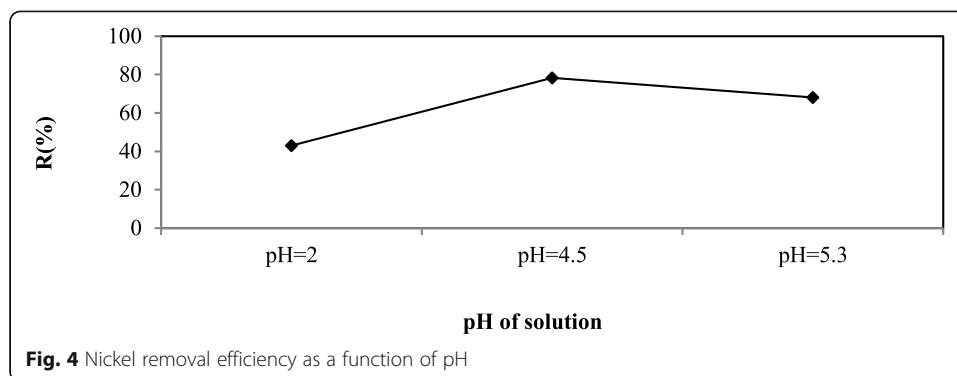
hydroxide ions in aqueous solution which decrease the adsorption yield [34]. Accordingly, pH = 4.5 value was selected as optimum pH for Ni(II) adsorption by BF slag in aqueous medium.

Effect of temperature

In adsorption processes, the temperature of the medium is a very influential parameter because it contributes to the fixation of metal ions on the surface of the adsorbent [35, 36]. The optimum temperature was set by realizing out adsorption tests at different temperatures (20.40 and 50 °C) under the following experimental conditions (C_0 30 mg/L; V_{ag} 200 rpm; pH 4.5; qe_{exp} 400 μm; M_{solid} 1 g), initial pH 4.9, agitation speed 200 rpm, adsorbent mass 1 g, initial concentration 30 mg/L, solid particle size 400 μm, and contact time 90 min (Fig. 5). The study of the temperature influence on the nickel adsorption has shown an inverse relationship between temperature and quantity of adsorbed ion, and it revealed that the adsorption is best at 20 °C (Figs. 5 and 6). Indeed, the nickel removal yield by BF slag between 20 and 40 °C, 20–50 °C, and 40–50 °C decreased respectively 16.8%, 21.96%, and 5.16% (Fig. 6).

From this study part, we deduced that the adsorption of nickel in aqueous solution by BF slag is exothermic [37]. The rise of the temperature of the medium has increased the resistance to mass transfer, and consequently, it slowed the diffusion of metal ions towards the surface of the adsorbent. This resistance could be due to the exothermic nature of adsorption processes of the nickel by BF slag [38].

Fig. 5 Effect of temperature

**Fig. 6** Nickel removal efficiency as a function of temperature

Effect of particle size

The adsorbent granulometry has an important role in the rate of transfer of metal ions from the solution to the adsorbent [39, 40]. In this work, we have varied the particle size of BF slag from 200 to 500 μm by following the same experimental protocol (C_0. 30 mg/L; V_{ag} 200 rpm; pH 4.5; T = 20 °C; M 1 g) (Fig. 7).

According to the experimental results conducted, it was noticed that when granulometry of the solid decreased from 500 to 300 μm, the amount adsorbed and yield respectively increased from 19.72 to 27.68 mg/g and 65.73 to 92.26% (Figs. 7 and 8). This means that the adsorption loses its effectiveness with the increase of the granulometry. This phenomenon is probably due to the narrowing of the specific surface of the adsorbent [41, 42]. It is important to clarify that with granulometry equal to 200 μm, we observed the decrease in the adsorption capacity and removal efficiency of 12.15 mg/g and 40.5% (Figs. 7 and 8). This result could probably be clarified by the emergence of the phenomenon of coalescence, that is to say the gathering of the particles of the adsorbent and the return to the upper diameters [42] (Figs. 7 and 8).

Effect of initial concentration

The nickel adsorption by BF slag in optimum conditions for different synthetic solutions has been studied. In this step, we noticed the evolution in the adsorbed quantity from 9.26 to 53.58 mg/g by varying the initial concentration from 10 to 100 mg/L (Fig.

Fig. 7 Effect of particle size
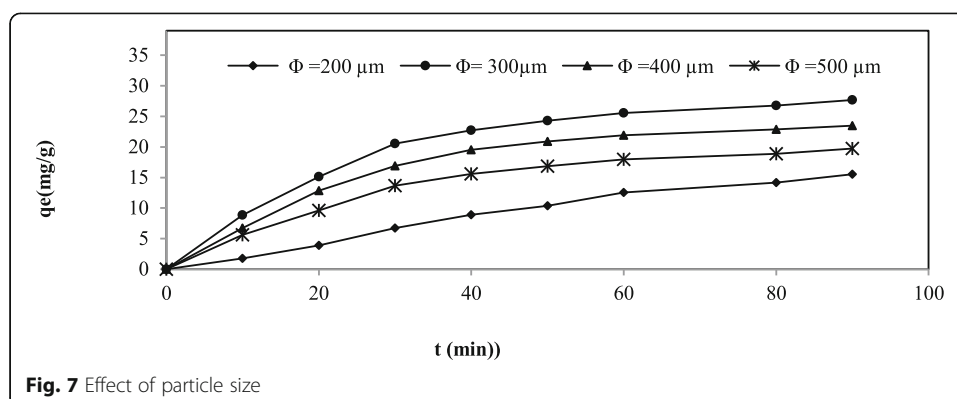
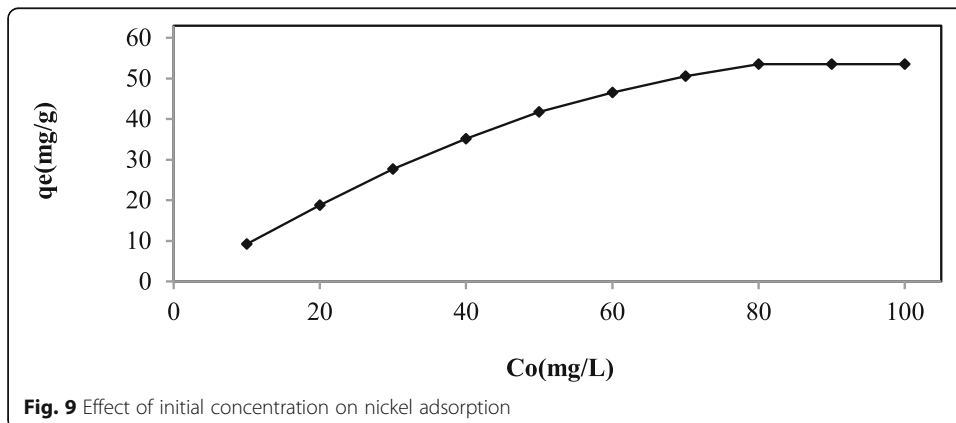**Fig. 8** Nickel removal efficiency as a function of particle size
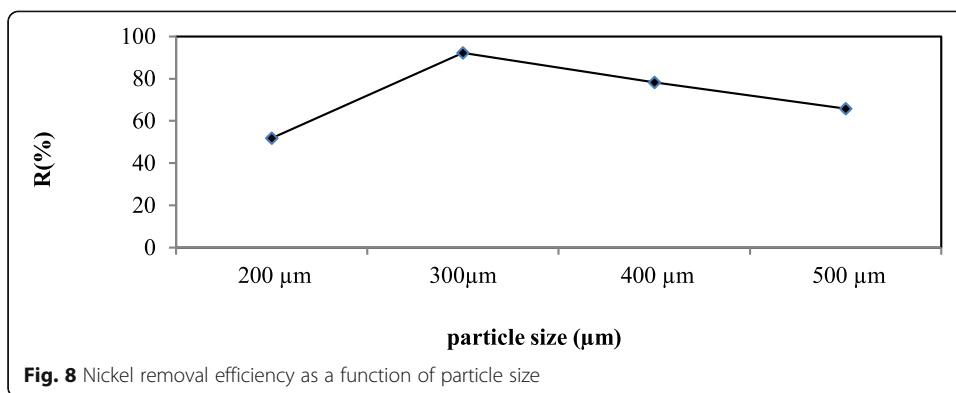
9). Indeed, as the initial concentration increases, the probability of contact between the adsorbent and the adsorbate per unit volume increased; therefore, the adsorbed amount increased [43, 44]. Nevertheless, the number of surface adsorption sites of the adsorbent material is limited; so, the adsorption capacity becomes constant [45–47]. Indeed, the plateau values showed that higher concentrations (> 80 mg/L) had no effect on the adsorption capacity and thus in the adsorption process.

The value of the adsorbed quantity at tier level is 53.58 mg/g. This result allows us to conclude that this quantity represents the maximum adsorption capacity, which can be fixed by 1 g of BF slag under our experimental conditions. It is important to indicate that at lower concentrations, the adsorption efficiency is higher due to the availability of vacant sites (Fig. 10).

Adsorption isotherm

The adsorption isotherm indicates the interaction between adsorbate and adsorbent, and it is brief to find the best fit in the adsorption process. In this study, the nickel adsorption by BF slag from the solution was fitted to both the Langmuir and Freundlich isotherm.

The Freundlich model is well adapted to describe the equilibrium in aqueous phase and describe that the multilayer adsorption is processed on a heterogeneous surface [48]. Its empirical formula is:

Fig. 9 Effect of initial concentration on nickel adsorption

Fig. 10 Nickel removal efficiency as a function of initial concentration
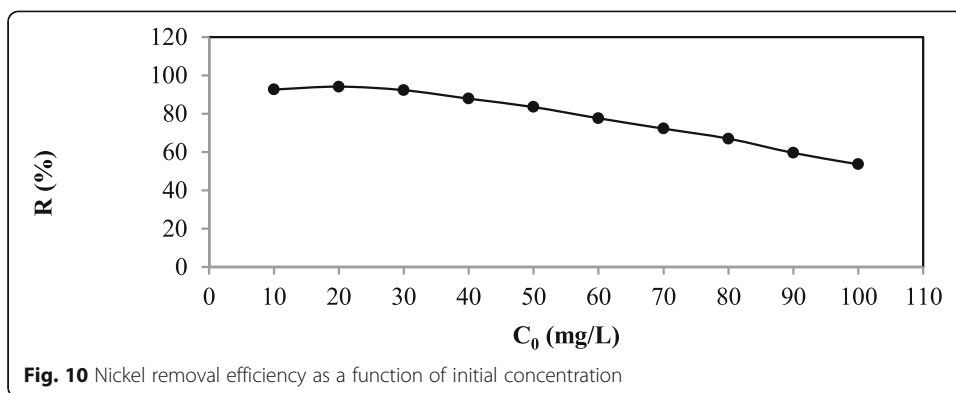
$$q_e = \frac{x}{m} = k.C_e^{1/n} \tag{3}$$

where q_e is the amount of adsorbate fixed at equilibrium by the adsorbent ($mg\,g^{-1}$), C_e is the residual concentration at equilibrium ($mg\,L^{-1}$), and K_F and $1/n$ are the Freundlich constants related to adsorption and affinity. The linearized Freundlich relation is written as follows:

$$\ln q_e = logk + \frac{1}{n}\ln C_e \tag{4}$$

The model of Langmuir [49] is most frequently employed to present the data on adsorption from solution. It is represented by the following equation:

$$q_e = \frac{b.q_m.C_e}{1 + b.C_e} \tag{5}$$

where q_e is the amount of adsorbent fixed at equilibrium by the adsorbent ($mg\,g^{-1}$), C_e is the residual concentration at equilibrium ($mg\,L^{-1}$), q_{max} is the maximum capacity ($mg\,g^{-1}$), and b is the thermodynamic constant of the adsorption equilibrium ($L.mg^{-1}$). The linear form of the Langmuir equation is shown as follows (Eq. 6):

$$\frac{C_e}{q_e} = \frac{1}{q_{max}}C_e + \frac{1}{q_{max}b} \tag{6}$$

The theoretical parameters of adsorption isotherms along with regression coefficients are listed in Table 2. Figures 11, 12, and 13 show the Langmuir model, Freundlich model, and adsorption isotherm of the nickel.

According to Fig. 13, the adsorption isotherms presented a classic appearance of a type I isotherm. The adsorption takes place gradually until it reaches a saturation level. According to the Table 2, the correlation coefficient value (R^2) of the Langmuir model was higher than that of the Freundlich model ($R^2_{Langmuir} = 0.99$, $R^2_{Freundlich} = 0.87$), and the value of nickel adsorption capacity obtained from the Langmuir model was

Table 2 Isotherm parameters nickel adsorption by BF slag

Freundlich model			Langmuir model		
K_F (mg.g^{-1})(ml.mg^{-1})$^{1/n}$	n	R^2	q_{max} (mg/g)	b (L.mg^{-1})	R^2
16.05	2.77	0.87	54.18	0.341	0.99

Fig. 11 Presentation of Freundlich model
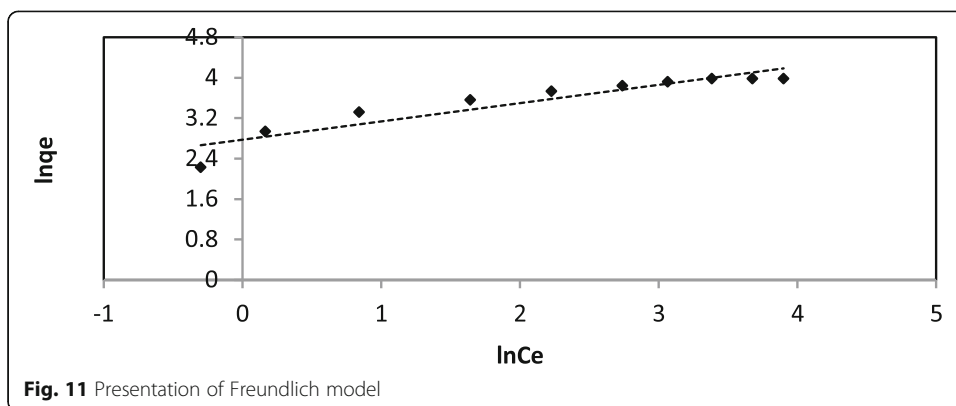
close to the experimental value. This implicate that the Langmuir equation was more appropriate to represent the process of nickel adsorption by BF slag in aqueous solution [23, 50].

According to Table 3, we also noticed that the value of the heterogeneity factor is between 1 and 10 (n = 2.77) which showed that the nickel absorption is favorable [51, 52].

The dimensionless R_L parameter is a feature of the Langmuir isotherm model that can illustrate the type of adsorption process [53, 54]. This parameter R_L is determined by the following equation:

$$R_L = \frac{1}{1 + C_0 b} \tag{7}$$

where b is the Langmuir isotherm constant, and C_0 is the initial concentration of solution.

The R_L values indicate the nature of the adsorption according to the following assumptions: favorable ($0 < R_L < 1$), unfavorable ($R_L > 1$), linear ($R_L = 1$), and irreversible ($R_L = 0$) [55, 56]. According to Fig. 14, we noticed that the values of the parameter R_L are between 0.237 and 0.03, which implies that the nickel adsorption process is favorable and follows a monolayer adsorption [56, 57]. According to Fig. 14, we noticed that
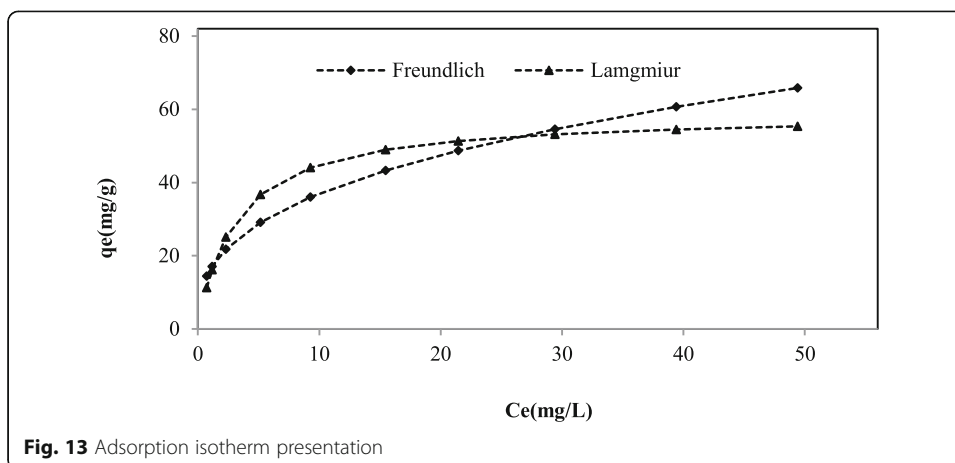

Fig. 12 Presentation of Langmuir model
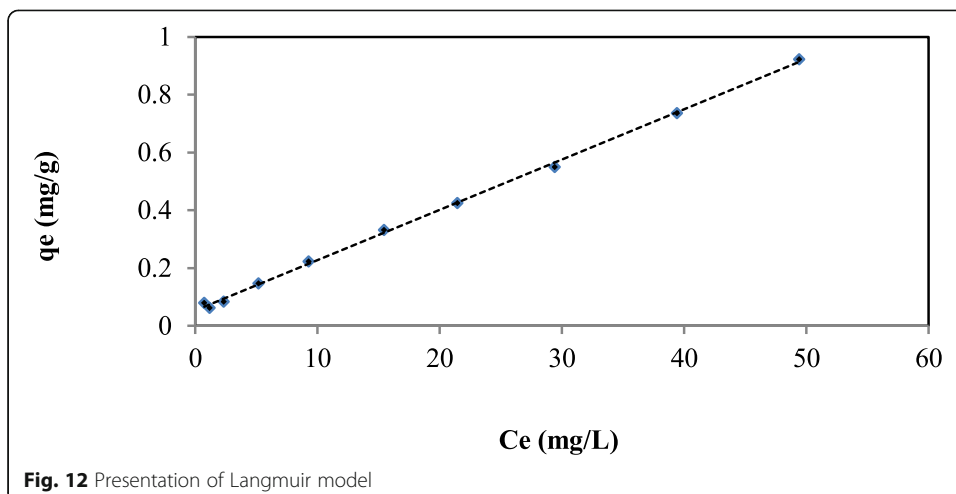
Fig. 13 Adsorption isotherm presentation

the values of the parameter R_L are between 0.237 and 0.03, which implies that the nickel adsorption process is favorable and follows a monolayer adsorption [56, 57].

Adsorption kinetics

The adsorption kinetics of nickel by the BF slag was investigated using pseudo-first-order and pseudo-second-order kinetics at different temperatures under optimal experimental conditions (Figs. 15 and 16). The pseudo-first-order model is represented by Lagergren equation [58]:

$$log(q_e - q) = -k_{Lag}t + log q_e \tag{8}$$

where q_e is the adsorbed quantity at equilibrium (mg/g), q is adsorbed quantity at time t (mg/g), and t is the time of adsorption process; in this study, it is from 0 to 90 min; k_{Lag} is the constant pseudo-first-order sorption speed (s^{-1}). The pseudo-second-order is represented by the Blanchard equation [59]:

$$\frac{t}{q} = \frac{1}{k_b q_e^2} + \frac{1}{q_e} \tag{9}$$

where q_e is the adsorbed quantity at equilibrium (mg/g), q is the adsorbed quantity at time t (mg/g), and t is the time of adsorption process; in this study, it is from 0 to 90 min; k_b is the constant of pseudo-second-order sorption speed (min^{-1}).

The curves obtained by fitting the pseudo-first-order and pseudo-second-order kinetics are presented in Fig. 15 and Fig. 16, respectively, and the relevant parameters are represented in Table 3.

Table 3 Kinetics data the nickel adsorption of by BF slag

T (°C)	qe_{exp} (mg/g)	Pseudo-first order			Pseudo-second order		
		K_{Lag} min^{-1}	qe_{theo} (mg/g)	R^2	K_b (mg/g.min)	qe_{theo} (mg/g)	R^2
20	27.68	0.040	28.58	0.96	0.00113	28.24	0.99
40	22.68	0.035	19.57	0.96	0.00139	23.09	0.99
50	18.27	0.052	26.86	0.95	0.00151	19.8	0.98

Fig. 14 Evolution of R_L ration as a function of initial concentration
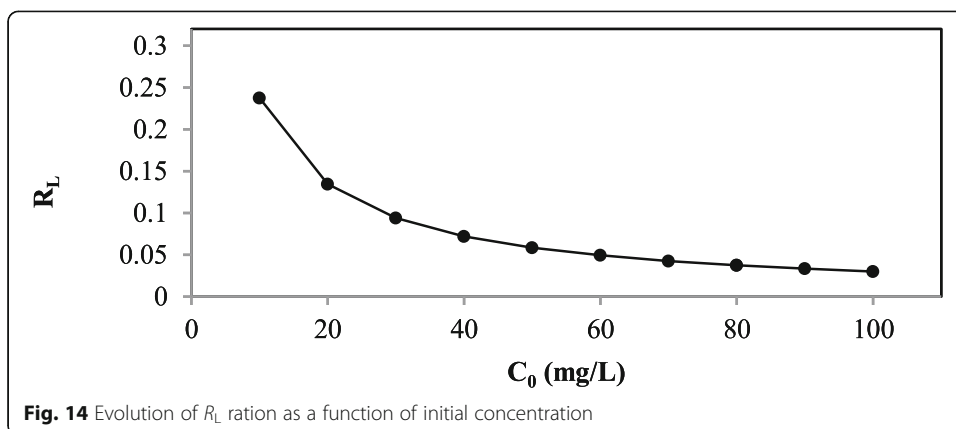
According to Table 3, the values of the correlation coefficients R^2 for the temperature studied were very high ($R^2 \geq 0.98$) for the Blanchard model; on the other hand, the values of the correlation coefficients of Lagergren model were less important $R^2 \geq 0.96$.

Also, the maximum values of the calculated adsorption capacity determined using the kinetic models were compared with experimental values. The results indicated the maximum adsorption capacity determined using the Blanchard model was closer to the experimental values. These results showed that the adsorption of nickel follows the kinetics of the pseudo-second-order model.

Adsorption mechanism

Weber and Morris [60] reported that if intra-particular scattering is involved in the sorption process, by increasing the adsorbed amount as a function of the square root of time, we need to obtain a line. This step is limiting if the line passes through the origin [61]. In the case where these lines do not pass through the origin, this indicates that the diffusion in the pores is not the only limiting mechanism of the sorption kinetics. It appears that other mechanisms are involved [62, 63]. The relation of Weber and Morris is presented as follows:
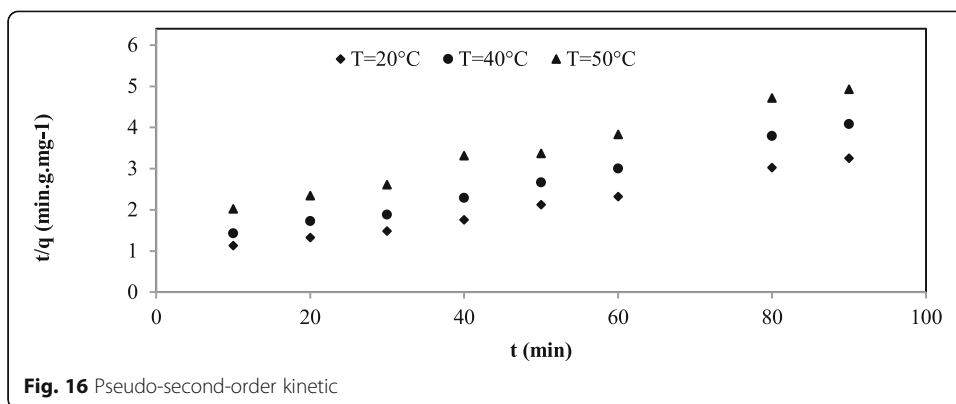
$$q = k_w \sqrt{t} + C \tag{10}$$

Fig. 15 Pseudo-first-order kinetic
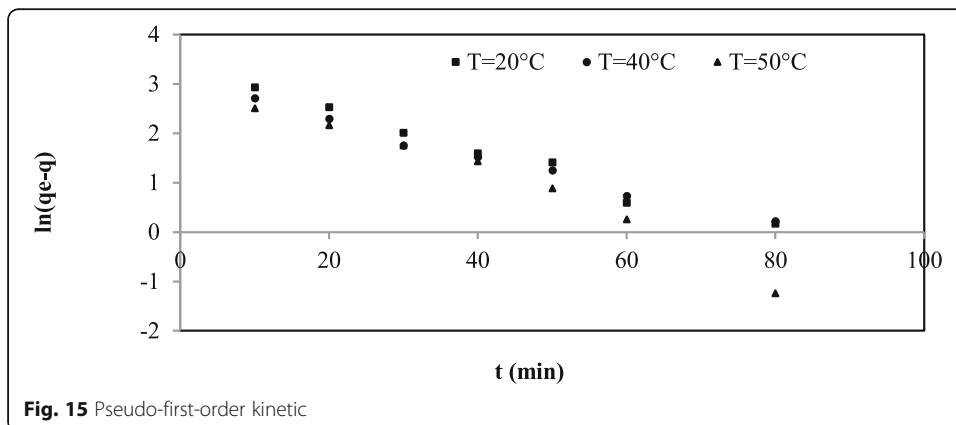
Fig. 16 Pseudo-second-order kinetic

where q is the quantity adsorbed at time t, t is the time measured in minute, k_w is the diffusion rate constant in the pores (mg/m. min $^{1/2}$), and C is the intercept .

K_w and C are obtained from the slope of the straight line of q versus $t^{1/2}$ (Fig. 17). The internal transport parameters values are represented from Table 4.

Optimization of kinetic data with the use of Weber and marries model confirmed that internal diffusion is not the main factor determining the process of nickel adsorption on BF slag (Fig. 17). Indeed, we noticed that the value of intercept is nonzero ($C \neq 0$). It is important to note that the larger the C value, the greater the influence of the boundary layer on adsorption, and the greater the dependence of the adsorption [64, 65]. This result allowed us to conclude that the adsorption process is controlled as the first step by the external transport, which is an instantaneous process followed by intra-particle diffusion [66, 67].

Thermodynamic study

The variations in standard free energy (ΔG), standard enthalpy (ΔH), and standard entropy (ΔS) were used to speculate on the adsorption mechanism. These thermodynamic parameters are calculated by utilizing the Equations 11, 12, and 13 [68–70]:
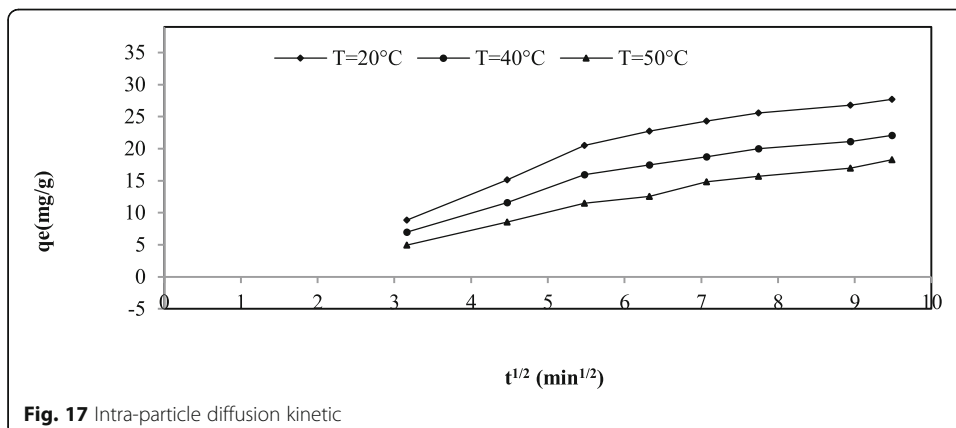
$$\Delta G^0 = -RTlnk_d \tag{11}$$

Fig. 17 Intra-particle diffusion kinetic

Table 4 Values of transport parameters

Temperature (°C)	The intercept	R^2	k_w (mg/g.min)
20	2.72	0.91	2.84
40	1.7	0.93	2.28
50	0.62	0.97	2.04

$$\ln k_d = \frac{\Delta H^0}{R} \times \frac{1}{T} + \frac{\Delta S^0}{R} \qquad (12)$$

The distribution coefficient is calculated from Equation 11 [71, 72].

$$k_d = \frac{C_i - C_e}{C_e} \times \frac{V}{M} = \frac{q_e}{C_e} \qquad (13)$$

Figure 18 shows the ln k_d versus 1/T plot for the adsorption of the nickel at different temperatures. The values of the thermodynamic parameters are grouped in Table 5. The negative value of Gibbs energy (ΔG) showed that the adsorption process is spontaneous and realizable [73, 74]. The negative value of the enthalpy variation (ΔH) indicates that the adsorption is exothermic and is physical in nature involving weak forces of attraction at solid/liquid interface [37, 75]. The value negative of entropy (ΔS) indicates a decrease in randomness at solid/liquid interface at the time of the nickel adsorption by BF slag surface [76, 77].

Conclusions

In this work, the nickel adsorption by BF slag from aqueous solution was investigated as a function of contact time, stirring speed, initial pH, temperature, particle size, and initial concentration in batch adsorption technique. The physico-chemical characterization showed that the adsorbent consists mainly of the silica, lime, and alumina. The specific surface area of the BF slag grains is of the order of 275.8 m^2/g. The optimization of the influencing parameters showed that the nickel removal efficiency and its maximum adsorption capacity, respectively, were 92.26% and 53.58 mg/g after 90 min of agitation. The kinetic studies showed that the mechanism of nickel

Fig. 18 Van't Hoff plot for nickel adsorption by BF slag
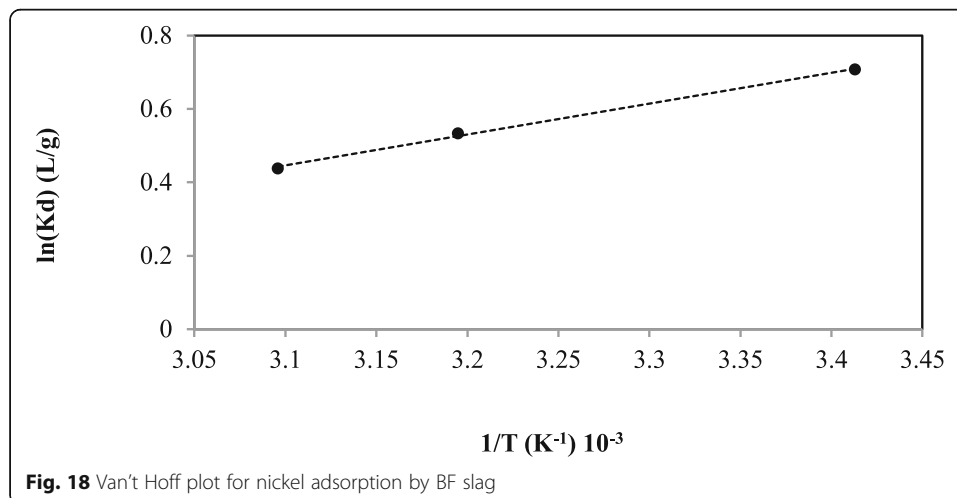
Table 5 Thermodynamic parameters of the nickel adsorption by BF slag

Temperature (K)	$\Delta H°$ (kj/mole)	$\Delta G°$ (kj/mole)	$\Delta S°$ (j/mole.K)	K_d (L/g)
293	− 6.988	− 12.949	− 17.962	2.028
313		− 13.381		1.704
323		− 13.552		1.549

adsorption process is well fitted by the pseudo-second order, the modeling results of kinetics indicated that the Langmuir model is more appropriate, and intra-particle diffusion is not the sole mechanism involved in this process. Thermodynamic study showed that the Ni(II) elimination by BF slag process is spontaneous, exothermic, and less entropic.

In conclusion, the results indicate that the BF slag represents a good adsorbent which can be used in the field of wastewater pollution control. Indeed, BF slag is better than the pyrophyllite, modified montmorillonite, raw red mud from aluminum industry, diatomite waste modified by EDTA, red mud, sea shells of Mehdia, and carbon aerogels [72, 78–83].

Abbreviations
BF slag: The blast furnace slag; CRTI : Research Center in Industrial Technologies; URASM: Iron and Steel Applied Research Unit; V_{ag}: Agitation speed; M_{solid}: Adsorbent mass; C_O: Initial concentration; $Ø_{solid}$: Adsorbent particle size; qe_{exp}: Maximum experimental absorbed capacity; qe: Amount of adsorbate fixed at equilibrium by the adsorbent; Ce: Residual concentration at equilibrium; K_F and $1/n$: The Freundlich constants related to adsorption and affinity; q_{max}: The maximum capacity; b: The thermodynamic constant of the adsorption equilibrium; k_{Lag}: The constant pseudo-first-order sorption speed; k_b: The constant of pseudo-second-order sorption speed; k_w: The diffusion rate constant in the pores; C : The intercept; K_d: The distribution coefficient; ΔG: Gibbs energy; ΔH: Enthalpy variation; ΔS: Entropy variation

Authors' contributions
TC conducted the research, analyzed the data, and wrote the paper; AB followed the experiences, and OK analyzed the data; all authors had approved the final version.

Availability of data and materials
All data generated or analyzed during this study are included in this published article [and its supplementary information files].

Declarations

Competing interests
The authors declare that they have no known competing financial interests or personal relationships that could have appeared to influence the work reported in this paper.

References
1. Fazio F, Piccione G, Tribulato K, Ferrantelli V, Giangrosso G, Arfuso F, Faggio C (2014) Bioaccumulation of heavy metals in blood and tissue of striped mullet in two Italian lakes. J Aquat Anim Health 26:278–284
2. Guan Q, Zhao R, Pan N, Wang F, Yang Y, Luo H (2019) Source apportionment of heavy metals in farmland soil of Wuwei, China: comparison of three receptor models. J Clean Prod 237:117792
3. Hamad QS, Muhamed SQ, Mohammed MQ (2020) Surface water pollution monitoring system based on IoT. Plant Arch 20:630–634
4. Vardhan KH, Kumar PS, Pand RC (2019) A review on heavy metal pollution, toxicity and remedial measures: current trends and future perspectives. J Mol Liq 290:111197
5. Villarín MC, Merel S (2020a) Assessment of current challenges and paradigm shifts in wastewater management. J Hazard Mater 390:122–139. https://doi.org/10.1016/j.jhazmat.2020.122139

6.   Zhou S, Yuan Z, Cheng Q, Zhang Z, Yang J (2018) Rapid in situ determination of heavy metal concentrations in polluted water via portable XRF: using Cu and Pb as example. Environ Pollut 243:1325–1333

7.   Xing W, Liu H, Banet T, Wang H, Ippolito JA, Li L (2020) Cadmium, copper, lead and zinc accumulation in wild plant species near a lead smelter. Ecotoxicol Environ Saf 198:110683

8.   Joshi, N., Sharma, Singh, A., (2017). Biosorption: a review on heavy metal toxicity and advances of biosorption on conventional methods. J Chem Chem Sci 7 (9): 714-724.

9.   Abdullah N, Yusof N, Lau WJ, Jaafar J, Ismail AF (2019) Recent trends of heavy metal removal from water/wastewater by membrane technologies. J Ind Eng Chem 76:17–38

10. Bolisetty S, Peydayesh M, Mezzenga R (2019) Sustainable technologies for water purification from heavy metals: review and analysis. Chem SocRev 48:463–487

11. Barakat MA (2011) New trends in removing heavy metals from industrial wastewater. Arab J Chem 4(4):361–377. https://doi.org/10.1016/j.arabjc.2010.07.019

12. Bashir A, Ahmad L, Sozia M, Taniya A, Mudasir M, Bhat A (2019) Removal of heavy metal ions from aqueous system by ion - exchange and biosorption methods. Environ Chem Lett 17:729–754

13. Chouchane T, Yahi M, Boukari A, Balaska A, Chouchane S (2016) Adsorption du cuivre en solution par le kaolin Adsorption of the copper in solution by the kaolin. J Mater Environ Sci 7:2825–2842

14. Chouchane T, Chouchane S, Boukari A, Mesalhi A (2015) Adsorption of binary mixture « Lead Nickel» by koalin. J Mater Environ Sci 6:924–941

15. Wang Y, Peng C, Padilla-Ortega E, Robledo-Cabrera A, López-Valdivieso A (2020) Cr (VI) adsorption on activated carbon: mechanisms, modeling and limitations in water treatment. J Environ Chem Eng 8:104031

16. Mohammadnezhad G, Abad S, Soltani R, Dinari M (2017) Study on thermal, mechanical and adsorption properties of amine-functionalized MCM-41/PMMA and MCM-41/PS nanocomposites prepared by ultrasonic irradiation. Ultrason Sonochem 39:765–773

17. Burakov AE, Galunin EV, Burakova IV, Kucherova AE, Agarwal S, Tkachev AG, Gupta VK (2018) Adsorption of heavy metals on conventional and nanostructured materials for wastewater treatment purposes: a review. Ecotoxicol Environ Saf 148: 702–712

18. Guerran ER, Aristizabal J, Arce B, Zurob E, Dennett G, Fuentes R, Suescún AV, Cardenas L, Rodrigues da Cunha TH, Cabezas R, García-Herrera C, Parra C (2021) Nanostructured Didymosphenia geminata-based membrane for efficient lead adsorption from aqueous solution Carolina Parra. J Environ Chem Eng 9(4):105269. https://doi.org/10.1016/j.jece.2021.105269

19. Mohd Syakirin MZ, Faradiella MK, Siti Nurjaliah M (2015) Adsorption of manganese in aqueous solution by steel slag, Procedia Environ. Sci. 30:145–150

20. Yusuf M, Chuah L, Khan MA, Choong TS (2014) Adsorption of nickel on electric arc furnace slag: batch and column studies. Sep Sci Technol 49:388–397

21. Sheng G, Yang S, Sheng J, Zhao D, Wang X (2011) Influence of solution chemistry on the removal of Ni(II) from aqueous solution to titanate nanotubes. Chem Eng J 168:178–182

22. Dhmees AS, Khaleel NM, Mahmoud SA (2018) Synthesis of silica nanoparticles from blast furnace slag as cost-effective adsorbent for efficient azo-dye removal, Egypt. J Petrol 27:1113–1121

23. Zhao H, Ouyang XK, Yang LY (2021) Adsorption of lead ions from aqueous solutions by porous cellulose nanofiber–sodium alginate hydrogel beads. J Mol Liq 324:115122

24. Taty-Costodes VC, Fauduet H, Porte C, Ho Y (2013) Removal of lead (II) ions from synthetic and real para la hidr´olisis enzim´atica de residuos lignocelul´osicos de yuca (Manihot esculenta Crantz). Rev Fac Ing Univ Antioquia 69(4)

25. Chidi O, Kelvin R (2018) Surface interaction of sweet potato peels (Ipomoea batata) with Cd (II) and Pb (II) ions in aqueous medium. Chem Int 4:221–229

26. Kumar PS, Gayathri R, Rathi S (2021) A review on adsorptive separation of toxic metals from aquatic system using biochar produced from agro-waste. Chemosphere 285:131438

27. El-Aassar MR, Mohamed FM (2021) Characterization valorized anthracite and its application in manganese (VII) adsorption from aqueous solution; batch and coluNi studies. Microporous Mesoporous Mater 310:110641

28. Niasri-Ghnimi S, Frini-Srasra N (2019) Removal of heavy metals from aqueous solutions by adsorption using single and mixed pillared clays. Appl Clay Sci 179:105151

29. Yu H, Covey GH, O'Connor AJ (2001) Effect of temperature and pH on the biosorption of ammonium onto posidonia oceanica fibers. Appita J 54:511–517

30. Jiang C, Wang X, Hou B, Hao C, Li X, Wu J (2020) Construction of a lignosulfonate-lysine hydrogel for the adsorption of heavy metal ions. J Agric Food Chem 68:3050–3060

31. Giewekemeyer K, Salditt T (2007) Counterion distribution near a monolayer of variable charge density. EPL Europhysics Lett 79(1):18003. https://doi.org/10.1209/0295-5075/79/18003

32. Penido ES, Melo LCA, Guilherme LRG, Bianchi ML (2019) Cadmium binding mechanisms and adsorption capacity by novel phosphorus/magnesium-engineered biochars. Sci Total Environ 671:1134–1143

33. Mahmoud ME, Yakout AA, Abdel-Aal H, Osman MM (2011) Enhanced biosorptive re- oval of cadmium from aqueous solutions by silicon dioxide nano-powder, heat inactivated and immobilized Aspergillus ustus. Desalination 279(1-3): 291–297. https://doi.org/10.1016/j.desal.2011.06.023

34. Mangaleshwaran L, Thirulogachandar A, Rajasekar V, Muthukumaran C, Rasappan K (2015) Batch and fixed bed column studies on nickel(II) adsorption from aqueous solution by treated polyurethane foam. J Taiwan Inst Chem Eng 55:112–118

35. Akltas D, Dizge N, Yatmaz HC, Caliskan Y, Ozay Y, Caputcu A (2017) The adsorption and Fenton behavior of iron rich Terra Rosa soil for removal of aqueous anthraquinone dye solutions: kinetic and thermodynamic studies, Water Sci. Technol. 76:3114–3125

36. El Aassar MR, Masoud MS, Elkady MF, Elzain AA (2018) Synthesis, optimization, and characterization of poly (Styrene-co-Acrylonitrile) copolymer prepared via precipitation polymerization. Adv Polym Technol 37:2021–2029

37. Foroutan R, Khoo FS, Ramavandi B, Abbasi S (2017) Heavy metals removal from synthetic and shipyard wastewater using Phoenix dactylifera activated carbon. Desalin Water Treat 82:1466156–1466156. https://doi.org/10.5004/dwt.2017.20908

38. Hodges SC, Johnson GC (1987) Kinetics of sulfate adsorption and desorption by Cecil Soil using miscible displacement. Soil Sci Soc Am J 51:323–331

39. Chen B, Sun W, Wang C, Guo X (2017) Size-dependent impact of inorganic nanoparticles on sulfamethoxazole adsorption by carbon nanotubes. Chem Eng J 316:160–170

40. Matsui Y, Nakao S, Sakamoto A, Taniguchi T, Shirasaki N (2015) Adsorption capacities of activated carbons for geosmin and 2-methylisoborneol vary with activated carbon particle size: effects of adsorbent and adsorbate characteristics. Water Res 85:95–102

41. Sekar M, Sakthi V, Rengaraj S (2004) Kinetics and equilibrium adsorption study of lead(II) onto activated carbon prepared from coconut shell. J Colloid Interface Sci 279(2):307–313. https://doi.org/10.1016/j.jcis.2004.06.042

42. Yogeshwaran V, Priya AK (2020) Adsorption of lead ion concentration from the aqueous solution using tobacco leaves. Materials Today: Proceedings 37:486–495. https://doi.org/10.1016/j.matpr.2020.05.467

43. Olgun A, Atar N (2012) Equilibrium, thermodynamic and kinetic studies for the adsorption of lead (II) and nickel (II) onto clay mixture containing boron impurity. J Ind Eng Chem 18:1751–1760

44. Rangan Mishra S, Chandra R, Kaila AJ, Darshi BS (2017) Kinetics and Isotherm studies for the adsorption of metal ions onto two soil types. Environ Technol Innov 7:87–101

45. Gupta N, Sen R (2017) Kinetic and equilibrium modelling of Cu (II) adsorption from aqueous solution by chemically modified Groundnut husk (Arachis hypogaea). Journal of Environ Chem. Eng. 5:4274–4281

46. Belbachir I, Makhoukhi B (2017) Adsorption of Bezathren dyes onto sodic bentonite from aqueous solutions, J. Taiwan Institute Chemi Engineers 75:105–111

47. Maleki MS, Moradi O, Tahmasebi S (2017) Adsorption of albumin by gold nanoparticles: equilibrium and thermodynamics studies, Arabian J. Chem. 10:S491–S502

48. Freundlich H (1906) Concerning adsorption in solutions. Z Phys Chem 57:385–470

49. Langmuir I (1908) The adsorption of gases on plane surfaces of glass, mica and platinum. J Am Chem Soc 40:361–403

50. Meshram YK, Gunjate JK, Khope RU (2020) Studies on adsorption characteristics of manganese onto coal based chemically modified activated carbon, Mater. Today: Proceedings 29:1185–1191

51. Erdem E, Karapınar N, Donat R (2004) The removal of heavy metal cations by natural zeolites. J Colloid Interface Sci 280: 309–314

52. Bensalah H, Younssi SA, Ouammou M, Gurlo A, Bekheet MF (2020) Azo dye adsorption on an industrial waste-transformed hydroxyapatite adsorbent: Kinetics, isotherms, mechanism and regeneration studies. J Environ Chem Eng 8: 103807

53. Goher ME, Hassan AM, Abdel-Moniem IA, Fahmy AH, Abdo MH, El-sayed SM (2015) Removal of aluminium, iron and manganese ions from industrial wastes using granular activated carbon and Amberlite IR-120H, Egypt. J Aquat Res 41: 155–164

54. Ayari F, Manai G, Khelifi S, Trabelsi-Ayadi M (2019) Treatment of anionic dye aqueous solution using Ti, HDTMA and Al/Fe pillard bentonite. Essay to regenerate the adsorbent. J Saudi Chem Soc 23:294–306

55. Weber TW, Chakravorti RK (1974) Pore and solid diffusion models for fixed-bed adsorbers. AICHE J 20(2):228–238. https://doi.org/10.1002/aic.690200204

56. Dubey R, Bajpai J, Bajpai AK (2016) Chitosan-alginate nanoparticles (CANPs) as potential nanosorbent for removal of Hg(II) ions. Environ Nanotechnol Monit Manage 6:32–44. https://doi.org/10.1016/j.enmm.2016.06.008

57. Mousa NE, Simonescu CM, Patescu RE, Onose C, Tardei C, Culita DC, Oprea O, Patroi D, Lavric V (2016) Pb^{2+} removal from aqueous synthetic solutions by calcium alginate and chitosan coated calcium alginate. React Funct Polym 109: 137–150

58. Lagergren S (1898) Zur theorie der sogenannten adsorption gelöster stoffe. Kungliga Svenska Vetenskapsakademiens, Handlingar 24:1–39

59. Haerifar M, Azizian S (2014) Fractal-like kinetics for adsorption on heterogeneous solid surfaces. J Phys Chem C 118(2): 1129–1134. https://doi.org/10.1021/jp4110882

60. Weber WJ, Morriss JC (1963) Kinetics of adsorption on carbon from solution. J Sanit Eng Div Am Soc Civ Eng 89:31–60

61. Ding L, Zou B, Gao W, Liu Q, Wang Z, Guo Y, Wang X, Liua Y (2014) Colloids and Surfaces A: Physicochem. Eng Aspects 446:1–7

62. Demiral H, Gündüzo-Glu G (2010) Removal of nitrate from aqueous solutions by activated carbon prepared from sugar beet bagasse. Bioresour Technol 101:1675–1680

63. Ofomaja AE (2010) Intraparticle diffusion process for lead(II) biosorption onto mansonia wood sawdust. Bioresour Technol 101(15):5868–5876. https://doi.org/10.1016/j.biortech.2010.03.033

64. Azarudeen RS, Ahmed MAR, Subha R, Burkanudeen AR (2015) Heavy and toxic metal ion removal by a novel polymeric ion-exchanger: synthesis, characterisation, kinetics and equilibrium. J Chem Technol Biotechnol 90:2170–2179

65. Gurses A, Hassani A, Kıransan M, Acıslı O, Karaca S (2014) Removal of methylene blue from aqueous solution using by untreated lignite as potential low-cost adsorbent: kinetic, thermodynamic and equilibrium approach. J Water Process Eng 2:10–21

66. Saleh TA (2015a) Nanocomposite of carbon nanotubes/silica nanoparticles and their use for adsorption of Pb(II): from surface properties to sorption mechanism. Desalin Water Treat 57(23):1–15. https://doi.org/10.1080/19443994.2015.1036784

67. Cheung WH, Szeto YS, McKay G (2007) Intraparticle diffusion processes during acid dye adsorption onto chitosan. Bioresour Technol 98:2897–2904

68. Zare EN, Lakouraj MM, Masoumi M (2018) Efficient removal of Pb (II) and Cd (II) from water by cross-linked poly (N-vinylpyrrolidone-co-maleic anhydride)@ eggshell/Fe_3O_4 environmentally friendly nano composite. Desalin Water Treat 106:209–219. https://doi.org/10.5004/dwt.2018.22104

69. Ahmadi A, Foroutan R, Esmaeili H, Tamjidi S (2020) The role of bentonite clay and bentonite clay@ MnFe2O4 composite and their physico-chemical properties on the removal of Cr (III) and Cr (VI) from aqueous media. Environ Sci Pollut Res Int 27:14044–14057

70. Saavedra LNM, Baeta BEL, Pereira MC, De Oliveira LCA, Da Silva AC (2017) Thermodinamic study of a magnetic molecular imprinted polymer for removal of nitrogenous pollutant from gasoline. Fuel. 210:380–389

71. Dehbi A, Dehmani Y, Omari H, Lammini A, Elazhari K, Abdallaoui A (2019) Hematite iron oxide nanoparticles (α-Fe 2 O 3): synthesis and modelling adsorption of malachite green. J Environ Chem Eng 8:103394
72. Fonseca-Correa RA, Giraldo L, Moreno-Piraján JC (2019) Thermodynamic study of adsorption of nickel ions onto carbon aerogels. Heliyon. 5:01789
73. Kamaraj R, Vasudevan S (2016b) Facile one-pot synthesis of nano-zinc hydroxide by electro-dissolution of zinc as a sacrificial anode and the application for adsorption of Th^{4+}, U^{4+}, and $Ce^{4}+$ from aqueous solution. Res Chem Intermed 42(5):4077–4095. https://doi.org/10.1007/s11164-015-2259-z
74. Diva TN, Zare K, Taleshi F, Yousefi M (2017) Synthesis, characterization, and application of nickel oxide/CNT nanocomposites to remove Pb2þ from aqueous solution. J Nanostruct Chem 7:273–281
75. Rajabzadeh M, Aghaie H, Bahrami H (2020) Thermodynamic study of Iron (III) removing by the synthesized a-Alumina powder and evaluating the corresponding adsorption isotherm models using Response Surface Method, Arabian. J Chemother 13:4254–4262
76. Kalhori EM, Yetilmezsoy K, Uygur N, Zarrabi M, Shmeis RMA (2013) Modeling of adsorption of toxic chromium on natural and surface modified lightweight expanded clay aggregate (LECA). Appl Surf Sci 287:4286442
77. Alalwan HA, Mohammed MM, J. Sultan A, Abbas MN, A. Ibrahim T, Aljaafari HAS, Alminshid AA (2021) Adsorption of methyl green stain from aqueous solutions using non-conventional adsorbent media: Isothermal kinetic and thermodynamic studies. Bioresour Technol Reports 14:100680
78. Scheidegger AM, Sparks DL, Fendorf M (1996) Mechanisms of nickel sorption on pyrophyllite: macroscopic and microscopic approaches, Soil Sci. Soc Am J 60:1763–1772
79. Ijagbemi CO, Baek MH, Kim DS (2010) Adsorptive performance of un-calcined sodium exchanged and acid modified montmorillonite for Ni2+ removal: equilibrium, kinetics, thermodynamics and regeneration studies. J Hazard Mater 174: 746–755
80. Smičiklas I, Smiljanić S, Perić-Grujić A, Šljivić-Ivanović M, Antonović D (2013) The influence of citrate anion on Ni (II) removal by raw red mud from aluminum industry. Chem Eng J 214:327–335. https://doi.org/10.1016/j.cej.2012.10.086
81. Sha H, Wu Y, Fan Y (2018) Utilization of industrial waste as a novel adsorbent: mono/competitive adsorption of chromium(VI) and nickel(II) using diatomite waste modified by EDTA. Appl Organomet Chem 32:e3977
82. Smiljanić S et al (2010) Rinsed and thermally treated red mud sorbents for aqueous Ni2+ ions. Chem Eng J 162:75–83
83. Allaoui M, Berradib M, Bensalah J, Es-sahbany H, Dagdag O, Ibn Ahmed S (2021) Study of the adsorption of nickel ions on the sea shells of Mehdia: Kinetic and thermodynamic study and mathematical modelling of experimental data. Materials Today: Proceedings 45:7494–7500

Publisher's Note